Chinese Journal of
POLYMER SCIENCE

ARTICLE

https://doi.org/10.1007/s10118-019-2299-8
Chinese J. Polym. Sci. **2020**, *38*, 53–62

Bio-based and Biodegradable Electrospun Fibers Composed of Poly(L-lactide) and Polyamide 4

Tao Chen[a,b,c*], Guo-Cheng Zhong[a,c], Yuan-Ting Zhang[a,c], Li-Ming Zhao[b,d], and Yong-Jun Qiu[b,d]

[a] *School of Materials Science and Engineering, East China University of Science and Technology, Shanghai 200237, China*
[b] *Key Laboratory of Bio-based Material Engineering of China National Light Industry Council, Shanghai 200237, China*
[c] *Shanghai Key Laboratory of Advanced Polymeric Materials, Shanghai 200237, China*
[d] *School of Biotechnology, East China University of Science and Technology, Shanghai 200237, China*

Electronic Supplementary Information

Abstract Novel bio-based and biodegradable block copolymers were synthesized by "click" reaction between poly(L-lactide) (PLLA) and polyamide 4 (PA4). Upon tuning the molar mass of PLLA block, the properties of copolymers and electrospun ultrafine fibers were investigated and compared with those of PLLA and PA4 blends. PLLA and PA4 were found incompatible and formed individual crystalline regions, along with reciprocal inhibition in crystallization. Electrospun fibers were highly hydrophobic, even if hydrophilic PA4 was the rich component. The crystallinity of either PLLA or PA4 decreased after electrospinning and PLLA-rich as-spun fibers were almost amorphous. Immersion tests proved that fibers of block copolymers were relatively homogeneous with micro-phase separation between PLLA and PA4. The fibrous structures of copolymers were different from those of the fibers electrospun from blends, for which sheath-core structure induced by macro-phase separation between homopolymers of PLLA and PA4 was confirmed by TEM, EDS, and XPS.

Keywords Poly(L-lactide); Polyamide 4; "Click" reaction; Electrospinning; Fiber

Citation: Chen, T.; Zhong, G. C.; Zhang, Y. T.; Zhao, L. M.; Qiu, Y. J. Bio-based and biodegradable electrospun fibers composed of poly(L-lactide) and polyamide 4. *Chinese J. Polym. Sci.* **2020**, *38*, 53–62.

INTRODUCTION

For decades, environmental concerns associated with petroleum-based polymers have aroused great attention in the field of biomass utilization. As the most popular candidate for environmentally friendly materials, poly(lactic acid) (PLA) is a typical bio-based thermoplastic polyester derived from 100% renewable resources and has significant potential due to its promising process ability, excellent mechanical properties, and biodegradability.[1–3] It has been extensively studied for use in several fields such as food industry and biomedical applications. Despite its excellent balance of properties, the use of PLA as a cost-effective alternative to commodity plastics has historically been limited by some drawbacks such as inherent brittleness, low heat deflection temperature, and intrinsically low crystallization rate.[4,5] In addition, lack of reactive functional groups on the backbone restricts the modification of PLA to improve its defects.[6] In the past years, copolymerization and blend with other polymers have been considered as efficient schemes to modify the bulk properties of PLA and to manufacture desirable materials.[7]

Polyamides are high performance engineering plastics with high strength and melting point. Besides traditional petrochemical-based polyamides, a series of bio-based polyamides such as PA11, PA610, and PA1010 have been developed from biomass materials.[8] The combination of bio-based polyester and polyamide can open avenues in design of new bio-based materials where polyester matrix benefits from the high thermal stability and high impact properties of polyamides.

Most researches focus on blends or copolymers of polyester and polyamide.[9,10] However, due to the poor compatibility between two kinds of polymers, a certain degree of macroscopic phase separation usually occurs in the blends,[10] thereby failing to improve performance. Their random copolymers, so-called poly(ester amide)s (PEAs), with properties between those of polyesters and polyamides have remarkable thermomechanical properties even at relatively low molecular weight, and the crystallinity and biodegradability can be regulated by changing the composition ratio.[11] Nakayama *et al*. reported that polyamide 4/poly(ε-caprolactone) (PA4/PCL) random copolymers could be well biodegraded at any composition ratio.[12] In most cases, random copolymerization will result in a broad molecular weight distribution and by-products that are difficult to be separated. For block copolymers of polyester and polyamide, they can express specific properties of each block rather than intermedi-

* Corresponding author, E-mail: tchen@ecust.edu.cn
Received March 22, 2019; Accepted May 20, 2019; Published online September 19, 2019

ate characteristics.[13] Gardella *et al*. designed PA11-*b*-PLA diblock copolymer without any macro-phase separation, and found fast stereocomplexation by mixing the enantiomeric diblock pairs.[14]

Although a variety of bio-based polyamides have been developed, they are not biodegradable and may be helpless to alleviate environmental pressures yet.[11,12] PA4, which has been extensively investigated over the last few years, can be synthesized from biomass substance by means of γ-aminobutyric acid or 2-pyrrolidone (PRN).[15,16] Moreover, it proved biodegradable in various environments such as soil,[17,18] seawater,[19] activated sludge,[20] and even *in vitro*.[21] Compounding PA4 with PLLA may provide a novel fully bio-based and biodegradable poly(ester amide)s. However, composite incorporating PLA and PA4 has rarely been reported. Kim *et al*. first reported a method with harsh condition for preparing poly(L-lactic acid)-block-polyamide 4 (PLLA-*b*-PA4), in which butyllithium, a flammable reagent, was used at −78 °C to substitute the end group of PLLA with PRN.[22] Biodegradation of this block copolymer was confirmed using lysozyme.

In this work, a new scheme was designed to prepare such fully bio-based and bio-degradable PLLA-*b*-PA4 copolymers by coupling PLLA and PA4 segments at room temperature using thiol-ene "click" reaction. It is highly efficient, moderate, and easy to carry out under light irradiation without metal catalyst.[23,24] Furthermore, ultrafine fibers were electrospun from synthesized PLLA-*b*-PA4. The chemical structure, thermal properties, and crystallization behaviors of PLLA-*b*-PA4 were examined, and the morphology, hydrophobicity, and structure of the electrospun fibers of PLLA-*b*-PA4 were analyzed and compared with those prepared from PLLA-SH/PA4 blends with the same composition, for which sheath-core fibers were electrospun directly through macro-phase separation without using coaxial electrospinning or emulsion electrospinning technique.

EXPERIMENTAL

Materials

L-lactide (L-LA, TCI, 98%) was recrystallized from dry ethyl acetate. 2,2′-Dithiodiethanol (DHEDS, TCI, 98%) and 2-pyrrolidone (PRN, biologically synthesized in our own laboratory) were used after distillation under vacuum. Tin(II) 2-ethylhexanoate (Sn(Oct)$_2$, Energy Chemical, 97%), tributyl phosphine (PBu_3, J&K, 98%), potassium *t*-butoxide (KTB, Aladdin, 99%), 10-undecenoyl chloride (Aladdin, 98%), and 2,2-dimethoxy-2-phenylacetophenone (DMPA, Aladdin, 99%) were used without further processing. Dichloromethane (DCM, Alfa Aesar, 99.5%) and hexafluoroisopropanol (HFIP, Meryer, 99.5%) were individually stored over molecular sieves. *n*-Hexane (Aladdin, 97%), methanol (Merck, ≥ 99.9%), formic acid (Aladdin, 99%) and acetone (Adamas, 99.9%) were used as received.

Preparation of PLLA-SS-PLLA

PLLA-SS-PLLAs containing an internal disulfide bond with various molecular weights were prepared by ring-opening polymerization of L-LA using DHEDS and Sn(Oct)$_2$ as initiator and catalyst, respectively. A typical synthetic step is as follows. Weighed L-LA, DHEDS, and Sn(Oct)$_2$ (0.2 wt% based on the weight of L-LA and dispersed in DCM) were added to a Schlenk flask under dry nitrogen flow. After removing DCM, the flask was sealed under vacuum and kept at 130 °C for 24 h. After that, the white product was dissolved in DCM and precipitated in cold methanol, and then dried in vacuum for 24 h.

Preparation of Thiolated PLLA

The thiolated PLLA (PLLA-SH) was synthesized by reducing PLLA-SS-PLLA as following. Predetermined amount of PLLA-SS-PLLA was completely dissolved in DCM in a Schlenk flask. After the exhausting-refilling process was repeated three times, 30-fold PBu_3 (with respect to the disulfide bond) was added quickly under a large amount of nitrogen purging. The mixture was shielded from light and stirred at room temperature for 60 min. The resulting solution was concentrated and poured into *n*-hexane. The precipitate was washed three times in methanol and then dried in vacuum at room temperature.

Preparation of Alkenylated PA4

The alkenylated PA4 was prepared using 10-undecenoyl chloride to initiate the ring-opening polymerization of PRN with KTB catalyst. In a typical procedure, weighed PRN and KTB were stirred under reduced pressure at 80 °C for 3 h. The temperature was then lowered to 50 °C and measured 10-undecenoyl chloride was added. After 24 h, the white product was dissolved in formic acid and precipitated in acetone for three times, and then dried under vacuum to a constant weight.

Synthesis of PLLA-*b*-PA4

The target PLLA-*b*-PA4 block copolymers were prepared by thiol-ene "click" reaction between PLLA-SH and alkenylated PA4. Alkenylated PA4 and 3-fold PLLA-SH (with respect to alkene group) were dissolved in HFIP and shielded from light under nitrogen gas. The reaction mixture was stirred until homogenization, and then added with 0.3-fold DMPA and purged with nitrogen for 10 min. Subsequently, the solution was exposed to 365 nm UV light for 15 min. The resulting solution was precipitated in a large excess of methanol. The precipitate was washed with DCM more than three times to remove unreacted PLLA-SH and then dried under vacuum to a constant weight. The copolymers are denoted as $PLLA_xPA4_y$, where *x* and *y* indicate the approximate number of repeating units of PLLA block and PA4 block, respectively.

Fabrication of Electrospun Fibers

The electrospun fibers of PLLA-*b*-PA4s and PLLA-SH/PA4 blends were prepared as follows. The polymers were dissolved in HFIP with a concentration of 13 wt%, and then drawn into a 10 mL syringe equipped with a stainless-steel needle (inner diameter of 0.24 mm). The solution was electrospun at a voltage of 25 kV at room temperature. The feed rate of the syringe was 1.5 mL·h^{-1}, and the distance between the needle tip and the collector plate was fixed at 12 cm. The resulting fibers were dried under vacuum at room temperature for whole night. For PLLA-SH/PA4 blend, the composition ratio was the same as that of the corresponding copolymer.

Characterization

Proton nuclear magnetic resonance (^{1}H-NMR) spectra of PLLA polymers in $CDCl_3$ and PA4 containing polymers in the mixture of $CDCl_3$ and CF_3COOD (4/3, *V*/*V*) were recorded on Bruker AVANCEIII 400MHz with TMS as internal standard. Differential scanning calorimetry (DSC) was conducted on a TA Q-2000

https://doi.org/10.1007/s10118-019-2299-8

thermal analyzer under a nitrogen flow of 20 mL·min^{-1} at a heating rate of 10 °C·min^{-1} from 0 °C to 275 °C. Wide angle X-ray diffraction (WAXD) was carried out on a Rigaku RINT2000 X-ray diffraction system operated at 40 kV and 100 mA with a nickel-filtered Cu-Kα radiation (λ = 0.154 nm) at room temperature, and scanned from 5° to 55°. Field emission scanning electron microscopy (SEM) measurements were carried out on a Hitachi S-4800 microscope. The average diameter and its distribution were estimated using an ImagePro Plus 6.0 analysis software. The surface contact angles of the electrospun fibrous membranes were measured on a contact angle meter at room temperature by sessile drop method using deionized water. The average roughness (R_a) of the electrospun membrane surfaces was obtained using tapping mode on a Park XE-100 atomic force microscope (AFM). The sheath-core structure of the fibers was characterized by transmission electron microscopy (TEM) on a Hitachi JEM-2100 microscope, and elements of the sheath layer were analyzed by an energy dispersive spectrometer (EDS) combined with TEM. The component of elements present on the fiber surface was also determined by X-ray photoelectron spectroscopy (XPS) on Thermo Scientific ESCALAB 250Xi, spectrometer.

RESULTS AND DISCUSSION

As shown in Scheme 1, the strategy for synthesizing PLLA-*b*-PA4 was designed on the basis of thiol-ene "click" reaction between PLLA-SH and alkenylated PA4. We selected thiol-ene "click" reaction to prepare PLLA-*b*-PA4 not only because it is easy to perform with high efficiency by UV irradiation at room temperature,[25] which can avoid hash reaction condition as reported, but also considering that the absence of metallic catalyst may provide potential utilization in medical material area. Furthermore, "click" reaction between different modularized blocks facilitates investigating the influence of various structural factors.

Synthesis of PLLA-SH

Establishing an effective and simple synthetic method for preparing thiol-functionalized (co)polymers has attracted much attention due to their wide usage in designing and synthesizing various bio-macromolecular structures. Typically, a "protection-deprotection" operation of the thiol-containing initiator is required before and after polymerization. But it can be avoided by taking reversible thiol/disulfide bond formation.[26,27] Here, as shown in Scheme 1(a), the disulfide initiator (DHEDS) was used to initiate ring-opening polymerization of L-LA to obtain a disulfide bond containing symmetric PLLA (PLLA-SS-PLLA). The disulfide bond was then reduced by a strong reductant (PBu_3) to produce thiolated PLLA (PLLA-SH).

Typical ^{1}H-NMR spectra of PLLA-SS-PLLA and corresponding reduction product PLLA-SH are shown in Figs. 1(a) and 1(b), respectively. The chemical shifts at 5.18 and 1.60 ppm were attributed to the protons of —C<u>H</u>— (1) and —C<u>H</u>$_3$ (5) of PLLA repeating units, respectively. After an efficient reduction, triple resonance signals at 2.92 ppm (4) attributable to —SSC<u>H</u>$_2$— of PLLA-SS-PLLA disappeared, along with a new quadruple resonance arising at 2.75 ppm (4′), assignable to HSC<u>H</u>$_2$— of thiolated PLLA-SH. Moreover, the signals at 4.39 ppm (3) belonging to methylene protons of —SSCH$_2$C<u>H</u>$_2$— in PLLA-SS-PLLA shifted to 4.25 ppm (3′) with a clear triple resonance signal after reduction. All these chemical shifts demonstrated the success of reduction reaction which conversed PLLA-SS-PLLA to PLLA-SH. The number-average molecular weights ($M_{n,NMR}$) of PLLA-SS-PLLA and PLLA-SH were estimated by calculating the ratio of integrated signal area of proton (1) (A_1) to that of protons (4) or (4′) (A_4 or $A_{4'}$) with Eqs. (1) and (2), respectively, and the results are listed in Table 1.

$$M_{n,NMR}(\text{PLLA-SS-PLLA}) = 288A_1/A_4 + 154 \quad (1)$$

$$M_{n,NMR}(\text{PLLA-SH}) = 144A_1/A_4 + 78 \quad (2)$$

In fact, it should be noted that the average numbers of repeating units of PLLA-SH were more than half of that of PLLA-SS-PLLA precursor. It might be attributed to that PLLA-SH fraction with lower molecular weight could be partially removed during the purification process of repeated precipitation.[26]

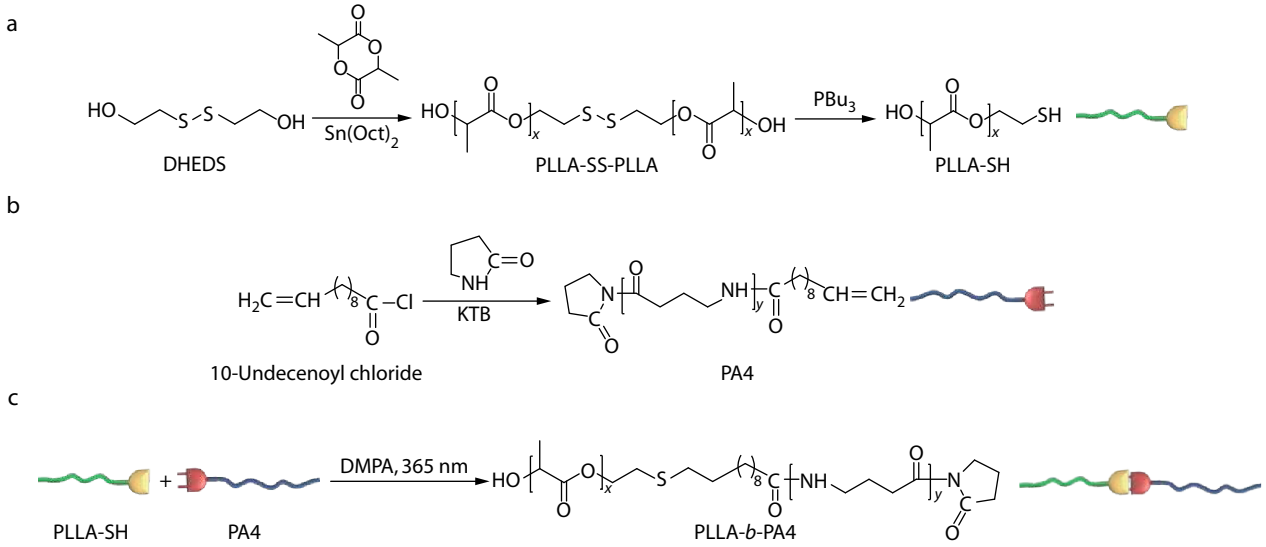

Scheme 1 The "click" reaction strategy for preparing PLLA-*b*-PA4 diblock copolymers: (a) synthesis of PLLA-SH, (b) synthesis of alkenylated PA4, and (c) synthesis of PLLA-*b*-PA4 by thiol-ene "click" reaction.

https://doi.org/10.1007/s10118-019-2299-8

Table 1 Reaction parameters and molecular weight of sulfur-PLLA and PA4.

Sample [a]	Monomer/initiator (mol/mol)	Yield (%)	$M_{n,NMR}$ [b] × 10^{-4} ($g \cdot mol^{-1}$)
$PLLA_{42}$-SS-$PLLA_{42}$	40	91	0.62
$PLLA_{119}$-SS-$PLLA_{119}$	208	85	1.73
$PLLA_{207}$-SS-$PLLA_{207}$	326	87	3.00
$PLLA_{42}$-SH	–	93	0.32
$PLLA_{119}$-SH	–	89	0.89
$PLLA_{207}$-SH	–	95	1.55
PA4	85	65	0.48

[a] The subscripts represent the approximate number of repeating units; [b] Determined from ^{1}H-NMR spectrum.

Synthesis of Alkenylated PA4

The synthetic route to alkenylated PA4 is shown in Scheme 1(b). Depending on the chemical structure of ene- and thiol-containing components, the reactivity of thiol-ene "click" reaction generally induced by photochemistry can vary significantly.[23] As indicated by Hoyle *et al*, the reactivity of ene group decreases as the electron density of the double bond decreases.[28] Therefore, 10-undecylenyl chloride was chosen as the initiator because its double bond is far away from the acyl chloride group. When it initiates the ring opening of PRN, the double bond at PA4 chain end can avoid the electron-withdrawing effect induced by amide bond and can ensure the "click" effi-

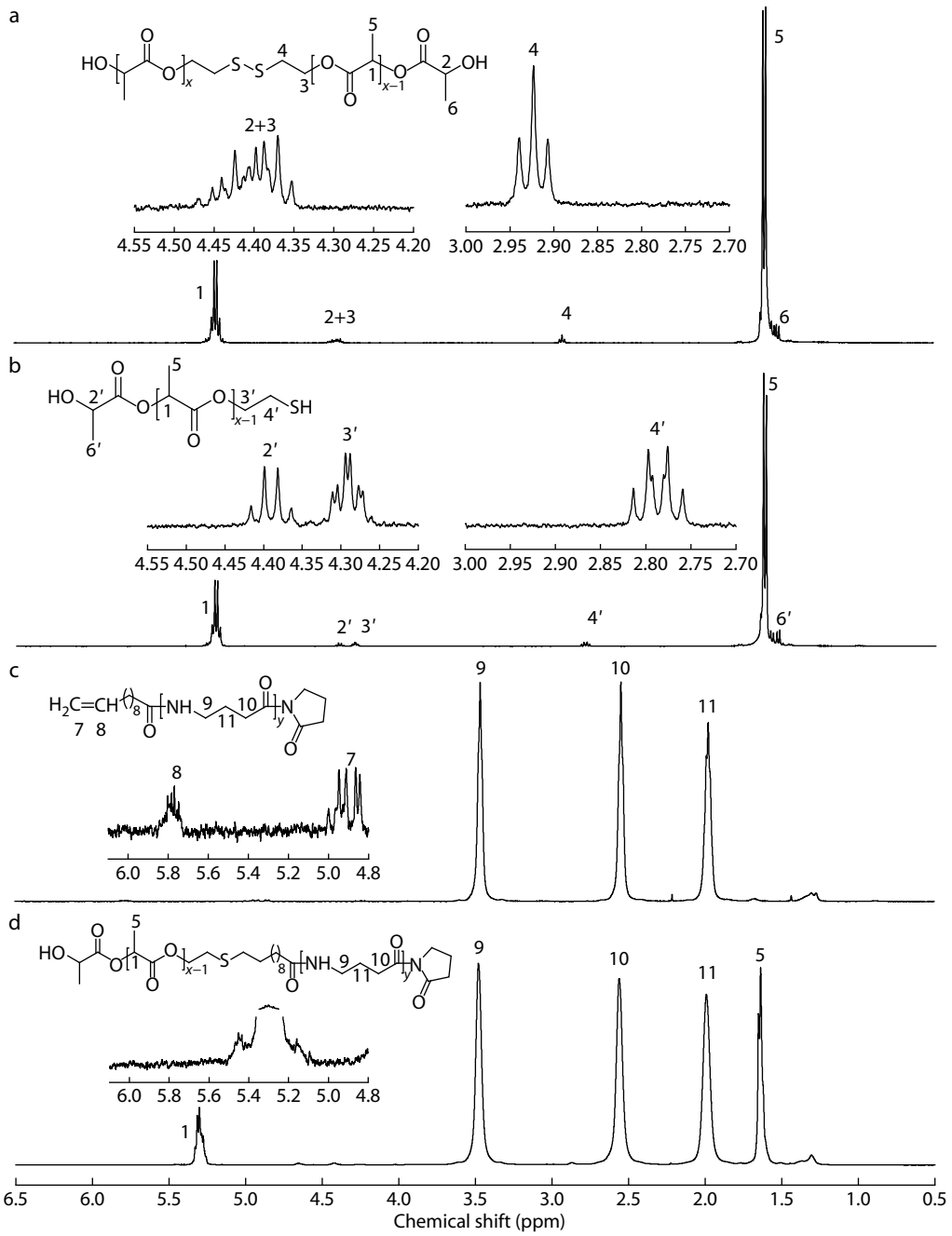

Fig. 1 ^{1}H-NMR spectra of (a) PLLA-SS-PLLA in $CDCl_3$, (b) PLLA-SH in $CDCl_3$, (c) alkenylated PA4 in TFA-d/$CDCl_3$, and (d) PLLA-*b*-PA4 copolymer in TFA-d/$CDCl_3$.

https://doi.org/10.1007/s10118-019-2299-8

ciency. A typical ^{1}H-NMR spectrum of PA4 with ene end group is shown in Fig. 1(c). Three major chemical shifts ranging from 2.08 ppm to 3.56 ppm (9, 10, and 11) were ascribed to the methylene protons of PA4 back bone. Moreover, the signals at 4.97 ppm (7) and 5.91 ppm (8) were attributed to the protons of $-C\underline{H}=C\underline{H}_2$ at the chain end. The results of ^{1}H-NMR analysis suggest the successful synthesis of alkenylated PA4. The number-average molecular weights ($M_{n,NMR}$) of PA4 was estimated by calculating the ratio of integrated signal areas of proton (9) (A_9) to that of protons (8) (A_8) with the formula of Eq. (3), and the result is listed in Table 1.

$$M_{n,NMR}(PA4) = 42.5A_9/A_8 + 251 \quad (3)$$

Synthesis of PLLA-*b*-PA4

As shown in Scheme 1(c), PLLA-*b*-PA4 block copolymers were achieved by thiol-ene "click" reaction between PLLA-SH and alkenylated PA4. Considering that the reactive groups were at the ends of long backbone, excess of PLLA-SH was applied to increase collision opportunity between reactive groups to ensure complete reaction of PA4. Fig. 1(d) displays the ^{1}H-NMR spectrum of PLLA-*b*-PA4, from which the proton signals of all repeating units of both blocks can be clearly recognized. Compared with spectrum (c) in Fig. 1, the proton signals of $-C\underline{H}=C\underline{H}_2$ at 4.97 ppm (7) and 5.91 ppm (8) disappeared on spectrum (d), demonstrating that PLLA-*b*-PA4 was successfully synthesized by thiol-ene "click" reaction. By comparing the integrated area values from signal (1) to signal (9) in spectrum (d), the ratio of PLLA to PA4 in PLLA-*b*-PA4 could be calculated and the molecular component of the block copolymer could also be estimated. Three well-defined PLLA-*b*-PA4 products with different ratios of 0.77, 2.00, and 3.33 were obtained and the molecular components are summarized in Table 2.

Table 2 Reaction yield and molecular component of PLLA-*b*-PA4.

Sample [a]	Yield (%)	Molar ratio of PLLA/PA4 [b]
$PLLA_{42}PA4_{54}$	72	0.77
$PLLA_{119}PA4_{54}$	67	2.00
$PLLA_{207}PA4_{54}$	57	3.33

[a] The subscripts indicate the approximate number of repeating units of each block; [b] Calculated by comparing the integrated area values of PLLA fragment to PA4 fragment from ^{1}H-NMR spectrum.

It should be pointed out that with the increasing PLLA-SH molecular weight, the yield of the final block copolymer decreased gradually from 72% to 57%. This might be due to that the corresponding steric hindrance of the functional group at chain end became large when the molecular weight of PLLA was increased, resulting in the reduction in "click" reaction efficiency.[29]

Thermal Properties and Crystallization Behaviors

Fig. 2 presents the DSC heating traces of $PLLA_{207}$-SH, PA4, and all PLLA-*b*-PA4 samples. Since the melting point of PA4 is around 265 °C, near its thermal decomposition temperature, the cooling trace is not available. For all samples, the glass transition is too weak to be discerned. The melting point, T_m, and the melting enthalpy, ΔH_m, of each block for different polymers are listed in Table 3. Each homopolymer presented its intrinsic melting peak. For copolymers, $PLLA_{42}PA4_{54}$ gave a sole T_m at 265.7 °C, attributed to PA4 block. No melting resonance of PLLA block could be examined for $PLLA_{42}PA4_{54}$. It suggests that PLLA block shorter than PA4 block kept amorphous in this copolymer. $PLLA_{119}PA4_{54}$ and $PLLA_{207}PA4_{54}$ both presented two melting peaks in the range of 157.9–163.9 and 262.0–263.3 °C, respectively assigned to PLLA and PA4 blocks. T_m of each block was lower than that of the corresponding homopolymer. With increasing PLLA content, T_m of PLLA block shifted to higher temperature near that of PLLA-SH, whereas for PA4 block, T_m successively decreased to 262.0 °C. ΔH_m of PLLA in each copolymer was smaller than that of neat PLLA-SH and the crystallinities calculated by the ratio of ΔH_m to ΔH_m^0, the melting enthalpy (93.7 J·g^{-1}) of the perfect crystallization, were lower than 14.7% (Table 3). Meanwhile, ΔH_m of PA4 block decreased from 72.6 J·g^{-1} to 28.8 J·g^{-1}. Although the quantitative crystallinity of PA4 block was unavailable due to lack of ΔH_m^0 value, the decrease in both T_m and ΔH_m still qualitatively indicates the decline in crystallinity of PA4. The results of DSC illustrate that both PLLA and PA4 blocks in copolymers could form individual crystalline regions, but the crystallization was mutually restricted. Extremely, the crystallization of short PLLA block could be remarkably constrained by the first-formed polyamide crystals.[14]

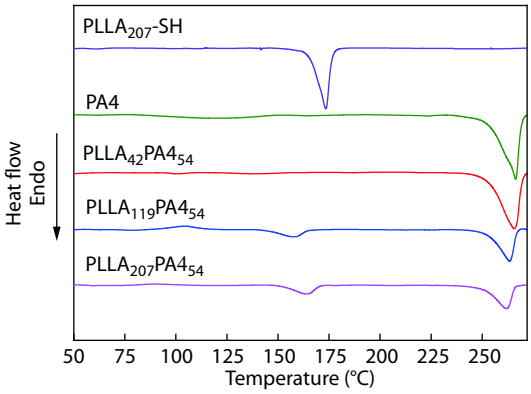

Fig. 2 DSC heat flow curves of $PLLA_{207}$-SH, PA4, and PLLA-*b*-PA4 copolymers in the first heating run.

Table 3 Thermal data of PLLA-*b*-PA4 determined by DSC in the first heating scan.

Sample	PLLA			PA4	
	T_m (°C)	ΔH_m (J·g^{-1})	f_w [a] (%)	T_m (°C)	ΔH_m (J·g^{-1})
$PLLA_{207}$-SH	166.8	52.1	55.6	–	–
$PA4_{54}$	–	–	–	266.0	72.6
$PLLA_{42}PA4_{54}$	–	–	–	265.7	58.4
$PLLA_{119}PA4_{57}$	157.9	9.4	10.0	263.3	32.9
$PLLA_{207}PA4_{57}$	163.9	13.8	14.7	262.0	28.8

[a] f_w represents the mass percentage crystallinity estimated by comparing ΔH_m to ΔH_m^0, the melting enthalpy of the perfect crystallization.

The crystalline structures of both blocks were determined by WAXD and the results are shown in Fig. 3. Typical diffraction peaks of PLLA-SH appeared at 2θ = 14.6°, 16.6°, 19.0°, and 22.3°, assigned to *α*-form crystals of PLLA, whereas the diffraction peaks of neat PA4 appeared at 20.5° and 24.2° also attributed to *α*-form crystals. As for copolymers, regardless of PLLA block length, there was neither shift nor new diffraction peaks arising, indicating no co-crystallization between PLLA and

PA4 blocks. The diffraction patterns of PA4 crystals always existed, along with the decline in relative intensity with increasing PLLA component. Contrarily, the diffraction peaks of PLLA did not appear until PLLA block was longer than PA4 block. Even so, the intensity of PLLA diffraction peaks was extremely weak. The absence of diffraction peaks of PLLA crystal from $PLLA_{42}PA4_{54}$ indicated that short PLLA block did not crystallize and remained amorphous, which agreed well with DSC results. The results of WAXD further proved that although each block of PLLA-*b*-PA4 crystallized individually within a certain component ratio, the crystallization was greatly restricted by each other, especially for PLLA block. It has been reported that in the same circumstances, the crystallization rate of PLA is usually slower than that of polyamide.[30] Although there is no exact data of crystallization rate of PA4, it can be presumed that the crystallization rate of PA4 should not be lower than those of other polyamides, since it has shorter repeating unit and corresponding higher hydrogen bond density. Therefore, it can be imaged that in the same condition, first-formed PA4 crystalline regions retarded the motion of PLLA blocks and restrained its crystallization. In extreme situation, short PLLA block was completely constrained by PA4 crystals and kept amorphous. All the results of DSC and WAXD confirm immiscibility between PLLA and PA4 blocks, and each one may maintain its individually intrinsic properties.

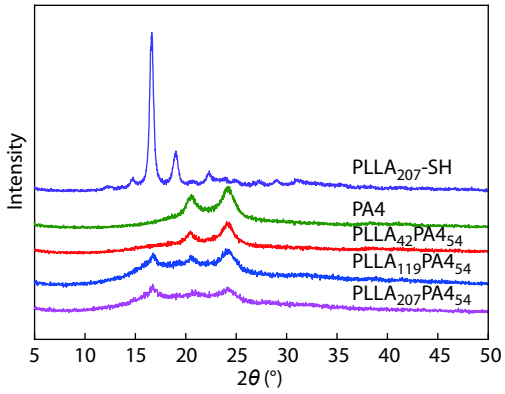

Fig. 3 WAXD patterns of $PLLA_{207}$-SH, PA4, and PLLA-*b*-PA4 powders.

Properties of Electrospun Fibers

In consideration of their biodegradable property and potential utilization, the prepared bio-based PLLA-*b*-PA4s were applied to electrospin ultrafine fibers and the fiber morphologies are presented as SEM photographs in Fig. 4, where the SEM images of electrospun fibers of $PLLA_{207}$-SH and $PA4_{54}$ and their blend are also shown. All as-spun fibers were smooth, ultrafine, and bead-free. The diameter distribution of all fibers shown in Fig. S1 (in the electronic supplementary information, ESI) suggested that the diameters of copolymer fibers followed unimodal distribution and the distribution of $PLLA_{119}PA4_{54}$ fiber diameter was the narrowest. The average diameters of $PLLA_{42}PA4_{54}$, $PLLA_{119}$-$PA4_{54}$, and $PLLA_{207}PA4_{54}$ were approximately 620 ± 61, 626 ± 38, and 850 ± 60 nm, respectively, depending only on PLLA block length since that of the PA4 block was fixed. Extending PLLA block length increased the overall molecular weight of the copolymers, which enhanced the chain entanglement in pre-spun solutions and eventually led to thicker diameter of the as-spun fibers.[31] The diameter of $PLLA_{207}$-SH fibers in Fig. 4(d) exhibited a very narrow distribution with the average value of 160 ± 11 nm (Fig. S1d, in ESI), only 1/5 of that of $PLLA_{207}PA4_{54}$ fibers. As for neat PA4 fibers in Fig. 4(e), bimodal distribution of diameter with 76 ± 14 and 594 ± 74 nm, respectively, was found in Fig. S1(e) (in ESI). Similar bimodal distribution of diameter was observed in Fig. S1(f) (in ESI) for fibers electrospun from blend of $PLLA_{207}$-SH and PA4. The average diameter of thin fibers was 88 ± 26 nm whereas of thick ones was 320 ± 22 nm, both smaller than those of fibers from their covalently bound copolymer $PLLA_{207}PA4_{54}$.

The hydrophobicity of as-spun fiber mat was evaluated by water contact angle test and the results are presented as insert pictures on the top right corner of each SEM image in Fig. 4. For electrospun fibers containing both PLLA and PA4, with increasing PLLA ratio, the water contact angle changed slightly from 125° ± 2° to about 137° ± 1°, exhibiting strong hydrophobicity similar to the neat $PLLA_{207}$-SH electrospun membrane whose water contact angle was 139° ± 1°. Although the water contact angle of the neat PA4 electrospun membrane was about 56° ± 3°, the existence of hydrophilic PA4 only slightly decreased the hydrophobicity of PLLA-containing membranes, which implies the domination of PLLA on

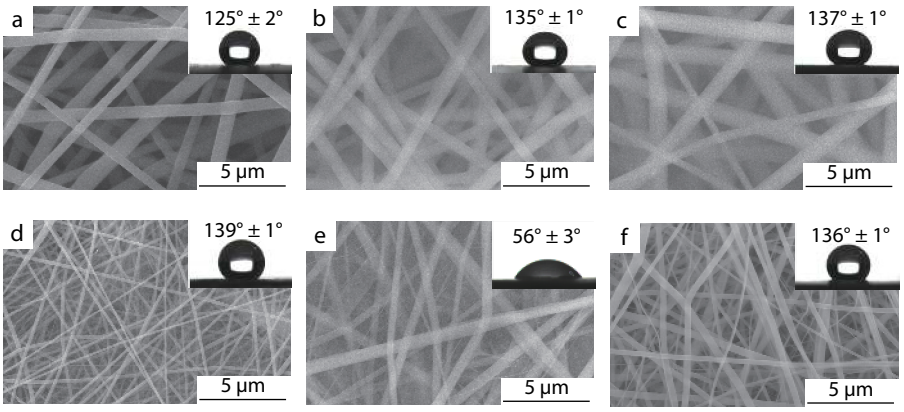

Fig. 4 SEM images of the electrospun fibers of (a) $PLLA_{42}PA4_{54}$, (b) $PLLA_{119}PA4_{54}$, (c) $PLLA_{207}PA4_{54}$, (d) $PLLA_{207}$-SH, (e) $PA4_{54}$, and (f) $PLLA_{207}$-SH/$PA4_{54}$ blend. The inserted graphs are the photographs of water droplets on the fibers for contact angle test.

https://doi.org/10.1007/s10118-019-2299-8

fiber hydrophobicity in current PLLA/PA4 ratio. In general, the thinning fibers would increase the roughness of membrane surfaces as verified by the results of AFM (see Fig. S2 in ESI), which should raise hydrophobicity of the surfaces and increase the contact angle. However, for PLLA-*b*-PA4 electrospun membranes in Figs. 4(a)–4(c), even the roughness of membrane surfaces increased with the decrease of fiber diameter caused by shorting PLLA length, the water contact angle decreased slightly rather than increased (see Fig. S2d in ESI). It indicated that the hydrophobicity of the electrospun membrane was mainly dominated by the composition of the fiber.

WAXD patterns of all electrospun fibers are shown in Fig. 5. Different from powder samples, the crystallinity of either PLLA or PA4 segment in electrospun fibers was very low. The as-spun $PLLA_{207}$-SH fibers were nearly amorphous without any diffraction peaks of PLLA crystal. In contrast, as-spun PA4 fibers presented weak characteristic diffraction peaks of *α*-form crystal at 20.5° and 24.2°, indicating a certain degree of crystallization. All as-spun PLLA-*b*-PA4 fibers were almost amorphous except that $PLLA_{42}PA4_{54}$ fibers had extremely weak diffraction peaks similar to those in the profile of neat PA4. The absence of PLLA diffraction peaks suggested that no PLLA crystal existed in all PLLA-containing copolymer fibers, even if PLLA was rich. Usually, the stretch of flow in the electric field might orientate the long chain and accelerate crystallization. The decrease in the crystallinity of each block was mainly due to the rapid evaporation of solvent that froze the motion of molecular chains and further retarded the crystallization.[32] However, the strong hydrogen bond interaction between PA4 units promoted regular alignment of PA4 segments.[33] On the other hand, hydrogen bonds also existed between PA4 and HFIP molecules, which slowed down the solvent evaporation from PA4-rich region.[34] Thus, when PA4 was rich, partial PA4 segments could adjust conformation to form crystals during electrospinning process. Nevertheless, when PLLA was rich, the alignment of PA4 was restricted and the fibers maintained amorphous. Hence crystalline peaks of neither PLLA nor PA4 could be observed, as indicated by Fig. 5.

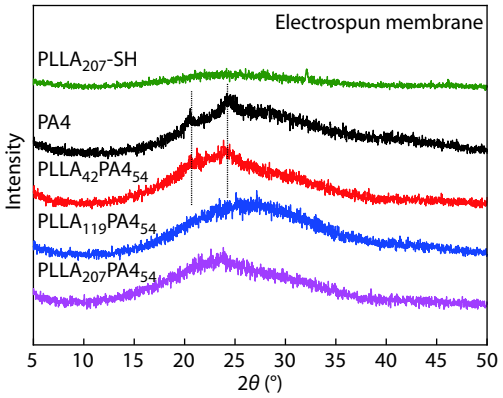

Fig. 5 WAXD patterns of electrospun fibers of $PLLA_{207}$-SH, PA4, and PLLA-*b*-PA4 copolymers.

In order to clarify fibrous structure, solvents that have no effect on PA4 were used to immerse the electrospun fibers. One is acetone, which cannot dissolve but swell PLLA segment. The fibers electrospun from PA4-rich and PLLA-rich copolymers were examined, and the fibers of blends with the same composition were also investigated as contrast. The SEM photographs of fibers after being immersed in acetone are shown in Fig. 6. All fibers still preserved the original structure after immersion. The fiber surface of $PLLA_{42}PA4_{54}$ with short PLLA block was smooth, while fibers of $PLLA_{207}PA4_{54}$ with long PLLA block exhibited rough surface with shallow grooves. As to fibers of blends, adhesion between fibers was observed after immersion. Especially for blend of $PLLA_{207}$-SH/$PA4_{54}$ with longer PLLA chain, the fiber surface was severely damaged. The results suggest that fibers electrospun from copolymers and blends might have different structures. For those from block copolymers, covalently bound PLLA and PA4 blocks homogeneously distributed in the fibers and only micro-phase separation would happen due to incompatibility between these two components. When immersed in acetone, only PLLA blocks on the surface were swollen and rearranged, leaving grooves on fiber surface. For PA4-rich block copolymer, the rearrangement of short PLLA block was prevented by PA4 micro-phase regions and non-distinct change on fiber could be observed. As to blends of these two incompatible homopolymers, macro-phase separation might take place in fibers and resulted in PLLA concentrated fiber surface.

To further verify the inference that phase separation between PLLA and PA4 in fibers of copolymers and blends took place at different scales, fibers were then immersed in DCM, a good solvent for PLLA but having no influence on PA4, and the results are presented in Fig. 7. The comparison with as-spun fibers in Fig. 4(a) and acetone immersed fibers in Fig. 6(a) revealed that DCM immersed $PLLA_{42}PA4_{54}$ fibers in Fig. 7(a) exhibited no significant change in either morphology or composition. As presented in Fig. 7(b), extending block length of PLLA led to serious adhesion between swollen fibers in DCM, ascribed to entanglement between long PLLA blocks. As for fibers from $PLLA_{42}$-SH/$PA4_{54}$ blend shown in Fig. 7(c), after being immersed in DCM, the diameter slightly reduced from 460 ± 56 nm of as-spun fibers to 350 ± 28 nm (Fig. S3 in

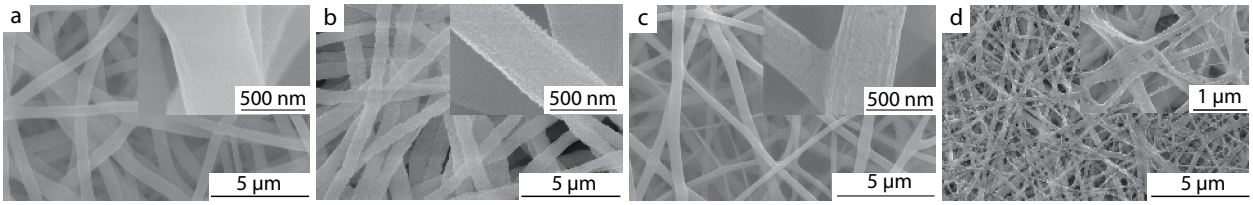

Fig. 6 SEM images of the electrospun fibers after immersing in acetone: (a) $PLLA_{42}PA4_{54}$, (b) $PLLA_{207}PA4_{54}$, (c) $PLLA_{42}$/$PA4_{54}$ blend, and (d) $PLLA_{207}$/$PA4_{54}$ blend.

https://doi.org/10.1007/s10118-019-2299-8

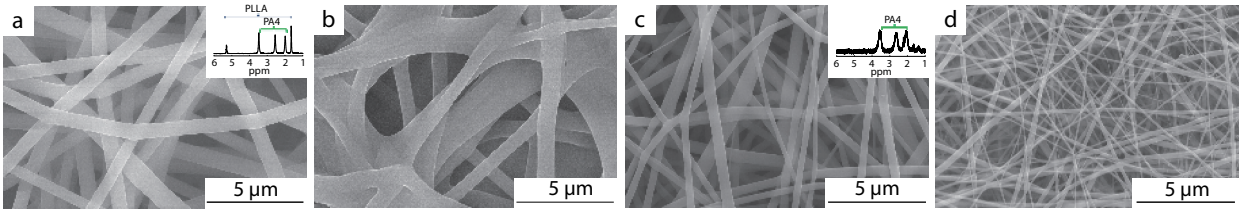

Fig. 7 SEM images of electrospun fibers after immersing in DCM: (a) $PLLA_{42}PA4_{54}$, (b) $PLLA_{207}PA4_{54}$, (c) $PLLA_{42}$-SH/$PA4_{54}$ blend, and (d) $PLLA_{207}$-SH/$PA4_{54}$ blend. The inserted graphs are ^{1}H-NMR spectra of corresponding fibers.

ESI) and the characteristic signals of PLLA component disappeared from ^{1}H-NMR spectrum. For fibers in Fig. 7(d) containing longer PLLA compared with that in Fig. 7(b), immersion in DCM resulted in distinct diameter reduction rather than adhesion between each fiber, along with signal disappearance of PLLA from ^{1}H-NMR spectrum. The bimodal distribution in diameter still remained after immersion, but the diameter reduced from about 320 ± 22 nm to 170 ± 29 nm and from 88 ± 26 nm to 35 ± 13 nm, respectively (Fig. S4 in ESI).

Shown in Fig. 8 are the typical results of TEM and EDS of $PLLA_{207}$-SH/$PA4_{54}$ as-spun fibers, which further disclosed the structure. Since it is difficult to clearly reveal the inner structure when the diameter of fibers exceeds 350 nm, only fibers with small diameter were randomly selected for observation. The sheath-core structure was corroborated from TEM image by obvious contrast between out sheath and inner core, but the core was not ideally located in the symmetry center of the fiber and resulted in heterogeneity of the sheath. The inlet red circle indicated the confines of sheath layer in TEM image for EDS analysis. The elements of C, O, Si, and Cu were detected. The strong signals of C and Cu arose from the carbon-coated copper whereas Si signal was escape peak. The absence of N proved that the sheath layer was predominantly composed by PLLA.

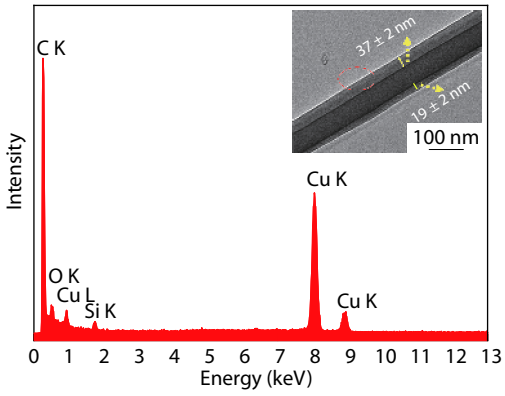

Fig. 8 TEM image and EDS spectrum of as-spun fibers of $PLLA_{207}$-SH/$PA4_{54}$ blend. The inlet circle within the confines of sheath layer was for EDS analysis.

For as-spun fibers from $PLLA_{42}$-SH/$PA4_{54}$ blend with the least PLLA content, the average diameter that exceeded 350 nm may cause low resolution in TEM observation and ambiguous EDS analysis. Therefore, XPS wide energy survey scans up to few nm depth on the fibers was performed to determine the elemental composition on the surface of as-spun fibers. The fibers of $PLLA_{42}PA4_{54}$ block copolymer were also examined as a contrast and the results are all illustrated in Fig. 9. The content of each element is summarized in Table 4. For $PLLA_{42}PA4_{54}$ block copolymer, the ratio of C:O:N of as-spun fibers obtained from XPS approximated to the theoretical atomic ratio (C: 63.96%, O: 25.88%, and N: 10.16%) as estimated from the number of repeating units of the copolymer, indicating homogeneous composition on fiber surface. However, a small amount of N element was detected by XPS from as-spun fibers of the blend. The intensity of N peak was only about 1/3 of that in copolymer fibers with the same composition. This can be ascribed to the low PLLA content induced thin or uncomplete sheath of some fibers in which PA4 core was exposed to a certain extent. After excluding such small part of PA4 component, the rest atomic ratio (C: 61.73%, O: 38.27%) approximated to the theoretical atomic ratio of $PLLA_{42}$-SH (C: 60.09%, O: 39.91%). Furthermore, detailed analysis of C 1s peaks in Fig. 9 proved that PLLA concentrated in sheath layer of as-spun fibers of $PLLA_{42}$-SH/$PA4_{54}$ blend (see Fig. S5 in ESI). The results of TEM, EDS and XPS verified the conclusion that the out surface of fibers electrospun from blend was mainly composed of PLLA due to macro-phase separation during electrospinning, different from that of copolymer fibers in which homogenous structure was formed.

All results suggested that the presence and absence of co-

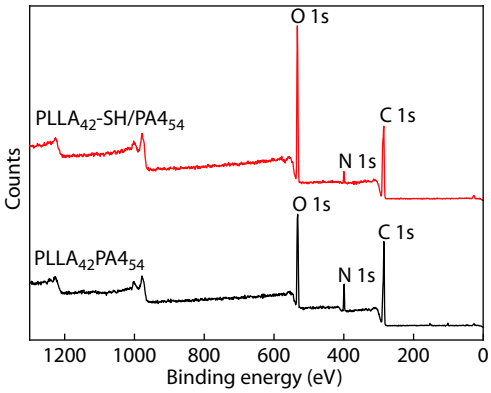

Fig. 9 XPS wide scans of $PLLA_{42}$-SH/$PA4_{54}$ blend and $PLLA_{42}PA4_{54}$ electrospun fibers.

Table 4 Atomic content obtained from XPS.

Fiber	Atomic (%)		
	C 1s	O 1s	N 1s
$PLLA_{42}PA4_{54}$	62.83	27.96	9.21
$PLLA_{42}$-SH/$PA4_{54}$	62.66	34.20	3.14

https://doi.org/10.1007/s10118-019-2299-8

valent bond between incompatible PLLA and PA4 segments had different effects on phase separation that occurred in the process of electrospinning fibers and resulted in various fibrous structures, as illustrated in Scheme 2. For block copolymers, only micro-phase separation took place due to the covalent bond between two incompatible blocks, and homogeneous fibrous structure was formed. When immersed in acetone, a poor solvent for PLLA and nonsolvent for PA4, only PLLA microdomain was affected and left defects on fiber surface. When immersed in good solvent for PLLA, such as DCM, adhesion between fibers took place due to dissolution of PLLA microdomain on fiber surface. As to blends of PLLA and PA4 without chemical bonding, the macro-phase separation between these incompatible polymers inevitably happened and led to sheath-core fibers. PA4 concentrated in inner core, while PLLA formed sheath layer, which was responsible for adhesion between fibers in acetone and sheath etching in DCM. Usually, fibers with sheath-core structure were obtained by emulsion or coaxial electrospinning technique. Current macro-phase separation induced sheath-core fibrous structure in common electrospinning process using single-nozzle technique from homogeneous solution may provide a new choice to conveniently prepare fibers with special structures.[35,36]

Although the degradative performance of neither PLLA-*b*-PA4 nor the electrospun fibers has been included here, the synthesized copolymers and the fibers constructed by PLLA and PA4 are naturally biodegradable due to the biodegradability of both components. In fact, it has been confirmed that PLLA-*b*-PA4 degraded in the presence of lysozyme and the degradation process was accelerated by increasing PLLA content due to deesterification.[22] Using either PA4 degrading microorganism or a lipase could improve the biodegradation of random copolyesteramides of 2-pyrrolidone and ε-caprolactone.[12] Furthermore, current results indicated that the diameter and distribution of electrospun fibers depended on not only the composition but also the chemical bonding between PLLA and PA4. Different diameters and diameter distributions of fibers usually lead to various specific areas and degradation rates. Therefore, the biodegradative performance of PLLA and PA4 contained fibers could be regulated by means of varying composition, chemical bonding, electrospinning condition, degradation environment and catalyst, or combining them, which may provide convenience to control the properties of such bio-based and biodegradable electrospun fibers for different utilizations.

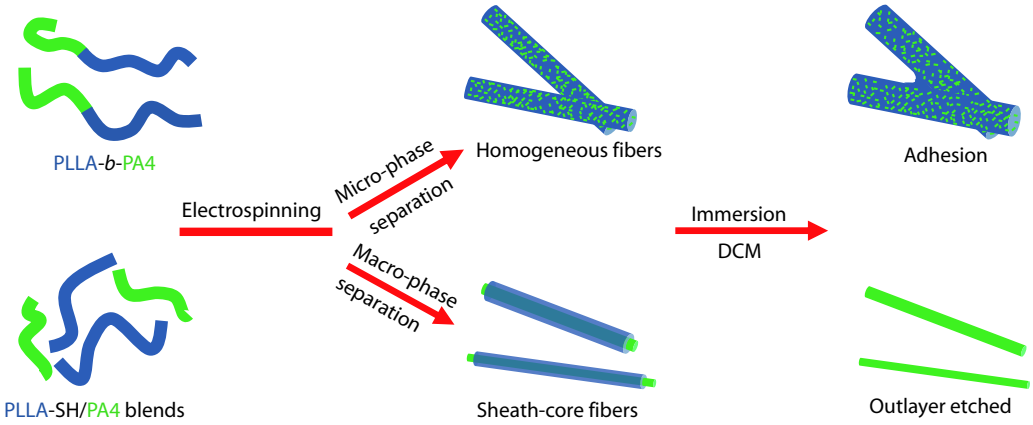

Scheme 2 Sketch of fibrous structures of block copolymers and blends.

CONCLUSIONS

In summary, PLLA-*b*-PA4 block copolymers with different composition ratios were conveniently synthesized by thiol-ene "click" reaction between thiolated PLLA and alkenylated PA4. PLLA and PA4 blocks were incompatible and formed individual crystalline regions, and the crystallization of each block was inhibited reciprocally. Ultrafine hydrophobic fibers were electrospun from either block copolymers or blends of PLLA and PA4. Fibers of PLLA-rich copolymers were almost amorphous and relatively homogeneous, along with micro-phase separation between two blocks. In contrast, due to lack of chemical bond, macro-phase separation took place during electrospinnin of PLLA and PA4 blends, leading to sheath-core fibers with PLLA mainly accumulated in the outlayer, as reported in previous articles. Since both components are fully bio-based and biodegradable, these novel fibers have promising potential applications in the fields of biomedical, packaging material, *etc*.

Electronic Supplementary Information

Electronic supplementary information (ESI) is available free of charge in the online version of this article at http://dx.doi.org/10.1007/s10118-019-2299-8.

ACKNOWLEDGMENTS

This work was financially supported by the National Key Research and Development Program of China (Nos. 2017YFB0309301 and 2017YFB0309302) and the Natural Science Foundation of Shanghai, China (No. 17ZR1407200). We are thankful to Dr. Feirong Gong for his help in this work.

REFERENCES

1 Drumright, R. E.; Gruber, P. R.; Henton, D. E. Polylactic acid technology. *Adv. Mater.* **2000**, *12*, 1841–1846.

2 Isono, T.; Kondo, Y.; Otsuka, I.; Nishiyama, Y.; Borsali, R.; Kakuchi, T.; Satoh, T. Synthesis and stereocomplex formation of star-shaped stereoblock polylactides consisting of poly(L-lactide) and poly(D-lactide) arms. *Macromolecules* **2013**, *46*, 8509–8518.
3 Li, T.; Zhang, J.; Schneiderman, D. K.; Francis, L. F.; Bates, F. S. Toughening glassy poly(lactide) with block copolymer micelles. *ACS Macro Lett.* **2016**, *5*, 359–364.
4 Kakroodi, A. R.; Kazemi, Y.; Nofar, M.; Park, C. B. Tailoring poly(lactic acid) for packaging applications *via* the production of fully bio-based *in situ* microfibrillar composite films. *Chem. Eng. J.* **2017**, *308*, 772–782.
5 Chen, L.; Hu, K.; Sun, S. T.; Jiang, H.; Huang, D.; Zhang, K. Y.; Pan, L.; Li, Y. S. Toughening poly(lactic acid) with imidazolium-based elastomeric ionomers. *Chinese J. Polym. Sci.* **2018**, *36*, 1342–1352.
6 Chiu, F. C.; Wang, S. W.; Peng, K. Y.; Lee, R. S. Synthesis and characterization of amphiphilic PLA-(P*α*N_3CL-*g*-PBA) copolymers by ring-opening polymerization and click reaction. *Polymer* **2012**, *53*, 3476–3484.
7 Rasal, R. M.; Janorkar, A. V.; Hirt, D. E. Poly(lactic acid) modifications. *Prog. Polym. Sci.* **2010**, *35*, 338–356.
8 Rogalsky, S.; Bardeau, J. F.; Wu, H.; Lyoshina, L.; Bulko, O.; Tarasyuk, O.; Makhno, S.; Cherniavska, T.; Kyselov, Y.; Koo, J. H. Structural, thermal and antibacterial properties of polyamide 11/polymeric biocide polyhexamethylene guanidine dodecylbenzenesulfonate composites. *J. Mater. Sci.* **2016**, *51*, 7716–7730.
9 Ge, Y. P.; Yuan, D.; Luo, Z. L.; Wang, B. B. Synthesis and characterization of poly(ester amide) from renewable resources through melt polycondensation. *eXPRESS Polym. Lett.* **2014**, *8*, 50–54.
10 Stoclet, G.; Seguela, R.; Lefebvre, J. M. Morphology, thermal behavior and mechanical properties of binary blends of compatible biosourced polymers: Polylactide/polyamide11. *Polymer* **2011**, *52*, 1417–1425.
11 Fonseca, A. C.; Gil, M. H.; Simões, P. N. Biodegradable poly(ester amide)s—a remarkable opportunity for the biomedical area: Review on the synthesis, characterization and applications. *Prog. Polym. Sci.* **2014**, *39*, 1291–1311.
12 Nakayama, A.; Yamano, N.; Kawasaki, N.; Nakayama, Y. Synthesis and biodegradation of poly(2-pyrrolidone-*co*-*ε*-caprolactone)s. *Polym. Degrad. Stab.* **2013**, *98*, 1882–1888.
13 Massimo, L.; Arturo, L. Q. M. Block copolymers as a tool for nanomaterial fabrication. *Adv. Mater.* **2003**, *15*, 1583–1594.
14 Gardella, L.; Mincheva, R.; De Winter, J.; Tachibana, Y.; Raquez, J. M.; Dubois, P.; Monticelli, O. Synthesis, characterization and stereocomplexation of polyamide 11/polylactide diblock copolymers. *Eur. Polym. J.* **2018**, *98*, 83–93.
15 Barnes, C. E. Nylon 4-development and commercialization. *Lenzinger Ber.* **1987**, *62*, 62–66.
16 Kawasaki, N.; Yamano, N.; Nakayama, A. Polyamide 4-block-poly(vinyl acetate) *via* a polyamide4 azo macromolecular initiator: thermal and mechanical behavior, biodegradation, and morphology. *J. Appl. Polym. Sci.* **2015**, *132*, 42466.
17 Tachibana, K.; Hashimoto, K.; Yoshikawa, M.; Okawa, H. Isolation and characterization of microorganisms degrading nylon 4 in the composted soil. *Polym. Degrad. Stab.* **2010**, *95*, 912–917.
18 Kazuhiko, H.; Tsuyoshi, H.; Masahiko, O. Degradation of several polyamides in soils. *J. Appl. Polym. Sci.* **1994**, *54*, 1579–1583.
19 Tachibana, K.; Urano, Y.; Numata, K. Biodegradability of nylon 4 film in a marine environment. *Polym. Degrad. Stab.* **2013**, *98*, 1847–1851.
20 Kawasaki, N.; Nakayama, A.; Yamano, N.; Takeda, S.; Kawata, Y.; Yamamoto, N.; Aiba, S. I. Synthesis, thermal and mechanical properties and biodegradation of branched polyamide 4. *Polymer* **2005**, *46*, 9987–9993.
21 Yamano, N.; Kawasaki, N.; Ida, S.; Nakayama, Y.; Nakayama, A. Biodegradation of polyamide 4 *in vivo*. *Polym. Degrad. Stab.* **2017**, *137*, 281–288.
22 Kim, J. W.; Kim, H. S. Synthesis and characteristics of poly(L-lactic acid-block-*γ*-aminobutyric acid). *Text. Sci. Eng.* **2015**, *52*, 53–58.
23 Lowe, A. B. Thiol-ene "click" reactions and recent applications in polymer and materials synthesis. *Polym. Chem.* **2010**, *1*, 17–36.
24 Li, M. Q.; Tang, Z. H.; Wang, C.; Zhang, Y.; Cui, H. T.; Chen, X. S. Efficient side-chain modification of dextran *via* base-catalyzed epoxide ring-opening and thiol-ene click chemistry in aqueous media. *Chinese. J. Polym. Sci.* **2014**, *32*, 969–974.
25 Liu, W.; Dong, C. M. Versatile strategy for the synthesis of hyperbranched poly(*ε*-caprolactone)s and polypseudorotaxanes thereof. *Macromolecules* **2010**, *43*, 8447–8455.
26 Hou, X.; Li, Q.; He, Y.; Jia, L.; Li, Y.; Zhu, Y.; Cao, A. Visualization of spontaneous aggregates by diblock poly(styrene)-*b*-poly(L-lactide)/poly(D-lactide) pairs in solution with new fluorescent CdSe quantum dot labels. *J. Polym. Sci., Part B: Polym. Phys.* **2009**, *47*, 1393–1405.
27 Kalarickal, N. C.; Rimmer, S.; Sarker, P.; Leroux, J. C. Thiol-functionalized poly(ethylene glycol)-*b*-polyesters synthesis and characterization. *Macromolecules* **2007**, *40*, 1874–1880.
28 Hoyle, C. E.; Lee, T. Y.; Roper, T. Thiol-enes: chemistry of the past with promise for the future. *J. Polym. Sci., Part A: Polym. Chem.* **2004**, *42*, 5301–5338.
29 Montañez, M. I.; Campos, L. M.; Antoni, P.; Hed, Y.; Walter, M. V.; Krull, B. T.; Khan, A.; Hult, A.; Hawker, C. J.; Malkoch, M. Accelerated growth of dendrimers *via* thiol-ene and esterification reactions. *Macromolecules* **2010**, *43*, 6004–6013.
30 Cho, A. R.; Shin, D. M.; Jung, H. W.; Hyun, J. C.; Lee, J. S.; Cho, D.; Joo, Y. L. Effect of annealing on the crystallization and properties of electrospun polylatic acid and nylon 6 fibers. *J. Appl. Polym. Sci.* **2011**, *120*, 752–758.
31 Baji, A.; Mai, Y. W.; Wong, S. C.; Abtahi, M.; Chen, P. Electrospinning of polymer nanofibers: effects on oriented morphology, structures and tensile properties. *Compos. Sci. Technol.* **2010**, *70*, 703–718.
32 Giller, C. B.; Chase, D. B.; Rabolt, J. F.; Snively, C. M. Effect of solvent evaporation rate on the crystalline state of electrospun nylon 6. *Polymer* **2010**, *51*, 4225–4230.
33 Schroeder, L. R.; Cooper, S. L. Hydrogen bonding in polyamides. *J. Appl. Polym. Sci.* **1976**, *47*, 4310–4317.
34 Zhang, P.; Tian, R.; Na, B.; Lv, R.; Liu, Q. Intermolecular ordering as the precursor for stereocomplex formation in the electrospun polylactide fibers. *Polymer* **2015**, *60*, 221–227.
35 Li, Y. J.; Chen, F.; Nie, J.; Yang, D. Z. Electrospun poly(lactic acid)/chitosan core-shell structure nanofibers from homogeneous solution. *Carbohyd. Polym.* **2012**, *90*, 1445–1451.
36 Zhang, J. F.; Yang, D. Z.; Xu, F.; Zhang, Z. P.; Yin, R. X.; Nie, J. Electrospun core-shell structure nanofibers from homogeneous solution of poly(ethylene oxide)/chitosan. *Macromolecules* **2009**, *42*, 5278–5284.

https://doi.org/10.1007/s10118-019-2299-8